Catalysis Communications 187 (2024) 106892

Contents lists available at ScienceDirect

Catalysis Communications

journal homepage: www.elsevier.com/locate/catcom

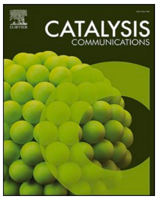

Influence of binder selection on the catalytic performance of zeolite-based bifunctional catalysts for biomass catalysis

Jinfei Lu [a,b], Shaohua Wang [a,b], Yanheng Hao [c], Lu Lin [d], Fan Bai [b], Wenhao Cui [e], Juan Wang [e], Qingda An [a,**], Peng Tian [e], Jifeng Pang [b,*], Wenhao Luo [b,c,*]

[a] School of Light Industry and Chemical Engineering, Dalian Polytechnic University, Dalian 116034, PR China
[b] CAS Key Laboratory of Science and Technology on Applied Catalysis, Dalian Institute of Chemical Physics, Chinese Academy of Sciences, Dalian 116023, PR China
[c] College of Chemistry and Chemical Engineering, Inner Mongolia University (Inner Mongolia), Hohhot 010021, PR China
[d] School of Materials Science and Engineering, Sun Yat-sen University, 135 Xingang Xi Road, Guangzhou 510275, PR China
[e] National Engineering Research Center of Lower-Carbon Catalysis Technology, Dalian National Laboratory for Clean Energy, Dalian Institute of Chemical Physics, Chinese Academy of Sciences, Dalian 116023, PR China

ARTICLE INFO

Keywords:
Catalyst binder
Bifunctional catalysts
Stability
Biofuels
Deactivation

ABSTRACT

The impact of binder selection on catalytic performance of real catalyst extrudates is still limitedly shown in biomass catalysis. Herein, we have prepared two zeolite-based bifunctional extrudates (Ni/LaY-Al_2O_3 and Ni/LaY-SiO_2). Compared with Ni/LaY-Al_2O_3, Ni/LaY-SiO_2 shows a markedly enhanced durability and sustained performance for 936 h in the continuous liquid-phase hydrogenation of γ-valerolactone into methyl pentanoate. Complementary characterization studies reveal that choosing SiO_2 as binder could efficiently mitigate metal agglomeration, coke formation and support dealumination during catalysis. These findings showcase that binder selection is essential for catalyst durability in the development of the industrial-level bifunctional catalysts for biomass valorization.

1. Introduction

The exhaustion of fossil resources, ever-increasing energy demands, and environmental problems promote the development of carbon-neutral chemicals or fuels to fulfill the stringent CO_2 emission regulations and goal of “carbon neutrality” [1–6]. Biomass is the only renewable carbon resource and has been regarded as an alternative raw material for the sustainable production of fuels and chemicals. Specifically, great efforts have been made to produce biofuels, which can efficiently abate CO_2 emissions in transportation sectors [6–10].

Pentanoic esters, mainly methyl or ethyl pentanoates, are recognized as apotential sort of biofuels in the transportation sector, as evidenced by the road trial of 250,000 km benefit from its outstanding compatibility with gasoline [11]. Pentanoic esters are usually derived from biomass-based levulinic acid (LA) via cascade reactions involving hydrogenation of LA to γ-valerolactone (GVL), ring-opening of GVL to pentenate ester (PEE) in the presence of alcohols and hydrogenation of PEE to pentanoic esters (Scheme 1) [12]. Among these, the reaction of ring-opening is the key step due to the relatively stable structure of GVL. Generally, bifunctional catalysts containing both metal centers and acid sites, such as Pd/MCM-41, Pd/ZSM-5, Ni/LaY, Ni/K-ZSM-5, Co@ZSM-5, Co/H-Y, Ru/SBA-SO_3H, Ru/H-ZSM-5, Ru/USY and Ru/LaY, were shown to be effective for the production of pentanoic esters [13–20]. Notably, our previous results show that the confined proximity between metal and acid sites could significantly enhance the catalytic performance in terms of activity and selectivity to pentanoic esters in the direct hydrogenation of ethyl levulinate to ethyl pentanoate over Ru/LaY catalysts in the batch system [18,21]. In the following work, a durable and economical Ni/LaY catalyst was developed for catalytic hydrogenation of GVL into pentanoic esters, with a sustained yield of ca. 90% towards pentanoic esters at 200 °C in 30 bar H_2 for 1000 h [19].

Extrusion molding by shaping zeolitic catalysts with binders is indispensable and pivotal for the industrial application [22,23]. The binders can not only facilitate to shape the catalyst material into various morphologies, but also improve the catalyst durability by enhancing the mechanical strength [24–26]. The introduction of a binder may vary the

---

* Corresponding authors at: CAS Key Laboratory of Science and Technology on Applied Catalysis, Dalian Institute of Chemical Physics, Chinese Academy of Sciences, Dalian 116023, PR China.
** Corresponding author.
E-mail addresses: anqd@dlpu.edu.cn (Q. An), jfpang@dicp.ac.cn (J. Pang), w.luo@dicp.ac.cn, w.luo@imu.edu.cn (W. Luo).

https://doi.org/10.1016/j.catcom.2024.106892
Received 15 January 2024; Received in revised form 26 February 2024; Accepted 1 March 2024

physic-chemical properties of the catalyst, and thus impact the performance during practical operations [27–29]. Still, the effect of binder selection on catalytic performance in particular for zeolite-based bifunctional catalysts is highly attractive yet rarely unraveled in biomass valorization, specially in the exploration of stable catalysts in a hydrogenation reaction under practical and long-term conditions.

In this work, we have tested the long-term performance of Ni/LaY-Al_2O_3 and Ni/LaY-SiO_2 in the hydrogenation of GVL into pentanoic biofuels, in the solvent of 45 wt% GVL in 45 wt% methanol and 10 wt% H_2O at $t = 200$ °C and $P_{H2} = 30$ bar in a fixed-bed reactor. Ni/LaY-SiO_2 shows outstanding catalyst durability, retaining a high methyl pentanoate (MP) yield of 92% even after a time on stream (TOS) of 936 h. Comparatively, Ni/LaY-Al_2O_3 experiences gradual deactivation within a TOS of 156 h. Further insights into the binder impact on the durability of bifunctional metal-acid catalysts have been disclosed by scanning transmission electron microscopy (STEM), temperature-programmed desorption of ammonia (NH_3-TPD), solid-state ^{27}Al magic angle spinning nuclear magnetic resonance measurements (^{27}Al MAS NMR) and X-ray photoelectron spectra (XPS).

2. Experimental section

2.1. Catalyst preparation

The commercial FAU-type zeolite La—Y (Si/Al = 2.7, 13.6 wt% La, Nankai University Catalysts Company, Tianjin, China) powder was first fully mixed with silica sol as SiO_2 precursor or pseudoboehmite as Al_2O_3 precursor, and subsequently was extruded into cylindrical catalysts with a diameter of 1 mm. The weight ratio of zeolite powder to the binder of SiO_2 or Al_2O_3 is 80:20. The shaped zeolite extrudates were first dried at 60 °C overnight, and then treated at 500 °C for 5 h in the air atmosphere.

Ni addition (10 wt%) into the LaY-Al_2O_3 or LaY-SiO_2 was further prepared by a wet impregnation method, as shown in Fig. S1 [19]. 50.56 g of $Ni(NO_3)_2 \cdot 6H_2O$ (98%, Aladdin) and 200 mL of H_2O were mixed into a 500 mL round-bottom flask, and further stirred for 30 min in a 50 °C water bath. Then, 90 g of as-prepared LaY-Al_2O_3 or LaY-SiO_2 extrudates, cut with a length of 1 mm, were added into the nickel precursor solution stepwise. The as-obtained mixture was heated to 60 °C and kept for 5 h with a slow stirring, and subsequently dried at 85 °C overnight. The obtained sample was heated to 450 °C (2 °C min^{-1}) and kept for 5 h under air flow. Prior to the reaction, the as-loaded catalyst extrudes were heated to 450 °C (2 °C min^{-1}) and kept 2 °C min^{-1} for 5 h in a 10 vol% H_2/Ar flow in the fix-bed reactor.

2.2. Characterizations

X'pert Pro X-ray diffractometer recorded the X-ray diffraction (XRD) patterns with monochromatic Cu Kα radiation, operating at a voltage of 40 kV and a current of 40 mA. The diffraction patterns were obtained between the range of 5° and 90°, while the step size was set at 0.0330°.

IRIS Intrepid II XSP instrument was employed for the inductively coupled plasma-optical emission spectroscopy (ICP-OES) to determine the actual Ni, Si, Al, and La contents over the Ni/LaY based catalyst. The spent catalysts were calcinated at 450 °C for 2 h under air flow (25 mL min^{-1}) to remove the coke before ICP-OES analysis.

Micromeritics ASAP-2460 instrument recorded the N_2 adsorption−desorption isotherms at −196 °C. All samples were treated under vacuum (10^{-3} Pa) at 350 °C for 12 h prior to the measurements.

JEOL JEM-2100F microscope recorded Scanning transmission electron microscopy (STEM) images at 200 kV. The composition and distribution of Ni, Si, and Al over the catalysts were analyzed on the energy dispersive X-ray analyzer equipped with the electronic microscope. Before characterizations, the catalysts were dispersed in ethanol, the up-layer solution was dropped on carbon-coated Cu grids for analysis.

Micromeritics AutoChem II 2920 chemisorption system equipped with a TCD detector recorded the temperature programmed desorption of ammonia (NH_3-TPD) spectra. Before measurement, about 100 mg catalysts were treated at 400 °C under He flow (25 mL min^{-1}) for 1 h. After cooling down to 100 °C, NH_3 was injected to reach adsorption saturation. The sample was heated up the sample to 600 °C (10 °C min^{-1}) under He flow and the signal of the desorbed NH_3 was detected by the TCD detector simultaneously. The amount of acid sites was calculated by integrating the area of desorption peak in NH_3-TPD profiles.

Thermal gravimetric (TG) spectra of the spent catalysts were tested by a TA Instruments SDT Q600 apparatus. The catalyst was first heated to 100 °C (10 °C min^{-1}) and kept for 60 min under air flow (25 mL min^{-1}) to exclude physically adsorbed H_2O. Then the catalyst was heated to 800 °C (10 °C min^{-1}) under air flow (25 mL min^{-1}) to remove the coke.

Solid-state ^{27}Al magic angle spinning nuclear magnetic resonance measurements (^{27}Al MAS NMR) (Bruker Advance III 400WB spectrometer) of catalysts were performed using a 4 mm DVT probe head. Rotors were set at 10 kHz and 104.28 MHz. For each single pulse experiment, 5000 scans were recorded and the corresponding relaxation delay and pulse width were 0.5 s and 0.77 μs, respectively. For a quantitative comparison, the acquired spectra were processed by Peak-Differentiation-Imitating-Analysis using Gauss function and the intensity of the center bands was integrated to give the relative quantification results.

X-ray photoelectron spectra (XPS) (Thermo SCIENTIFIC ESCALAB 250 Xi spectrometer) were collected with a monochromated Al Kα radiation (hυ = 1486.6 eV). All the obtained XPS spectra were calibrated by the adventitious carbon C *1s* band (284.6 eV).

2.3. Catalyst testing

Catalyst stability tests were performed in a continuous flow system with a tubular stainless-steel reactor (16 mm inner diameter, as shown in Fig. S2). The catalyst (3 mL) was loaded between two quartz wool plugs with 3 mL quartz sand on both sides. The catalyst was first reduced at 400 °C under a H_2 flow (30 bar, 40 mL min^{-1}) for 1 h and then cooled to the 200 °C. The feedstock (45 wt% GVL in 45 wt% methanol and 10 wt% H_2O) was pumped into the reactor with a weight hour space velocity (WHSV) of 1 h^{-1}. The final products were detected by a gas chromatograph (Agilent 7890 A) equipped with an HP-5 column (30 m × 0.32 mm × 0.25 μm) and a flame ionization detector (FID).

The calculation equations of GVL conversion and methyl pentanoate (MP) yield are as follows:

$$\text{GVL conversion } (\%) = (\text{moles of inlet GVL–moles of outlet GVL}) / \text{moles of inlet GVL} \times 100\%$$

$$\text{MP yield } (\%) = \text{moles of EP produced/moles of inlet GVL} \times 100\%$$

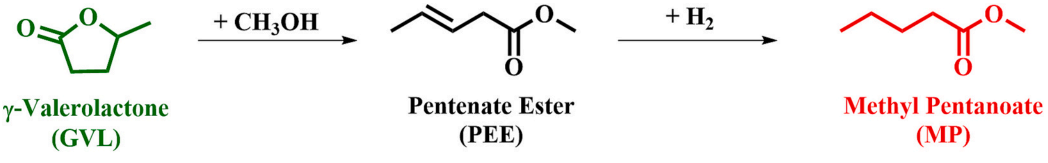

Scheme 1. Schematic illustration of the hydrogenation of γ-valerolactone into methyl pentanoate.

3. Results and discussion

3.1. *Physical properties of Ni/LaY-Al_2O_3 and Ni/LaY-SiO_2 catalysts*

Two Ni/LaY-Al_2O_3 and Ni/LaY-SiO_2 catalysts were successfully prepared and applied for the hydrogenation of GVL to MP. Both fresh and spent catalysts were first characterized by XRD. As shown in Fig. 1, besides the feature peaks of zeolite Y, a distinct peak at 2θ angle of 44.5, assigned to the (111) plane of Ni (PDF#04–0850), could be detected for all the catalysts [30,31]. According to the Scherrer equation at the 2θ value of 44.5°, the average diameters of Ni particles on the fresh Ni/LaY-Al_2O_3 and Ni/LaY-SiO_2 were similar and around 22 nm. After the continuous catalytic reactions, a large difference in the change of the average Ni particle size can be observed for the spent catalysts. The average Ni particle size of the spent Ni/LaY-Al_2O_3 increases to 38.5 nm markedly after a time-on-stream (TOS) of 156 h, while that of the spent Ni/LaY-SiO_2 just shows a limited change to 26.5 nm even after a TOS of 936 h. This points should be attributed to the strong impact of the binder on metal agglomeration during catalysis.

The contents of metal loading and porous properties of the fresh and spent catalysts are shown in Table 1. For the fresh Ni/LaY-Al_2O_3 and Ni/LaY-SiO_2 catalysts, the Ni and La contents were similar and around 8.1–8.2 % and 8.2–8.4%, respectively, in line with their theoretical contents in catalysts. Notably, an obvious change in the Al content from 18.5% for the fresh Ni/LaY-Al_2O_3 to 15.9% for the spent Ni/LaY-Al_2O_3 is observed, indicating support dealumination when using alumina as the binder under the hydrothermal conditions. In contrast, no apparent Al loss is observed for Ni/LaY-SiO_2 even after a TOS of 936 h, demonstrating the excellent durability of the catalyst when using silica as the binder. Additionally, the surface area of Ni/LaY-Al_2O_3 undergoes an obvious decline from 481 to 378 m^2 g^{-1} after catalysis, mainly attributed to the more carbon residue on the catalyst. Differently, Ni/LaY-SiO_2 catalysts only perform a slight decrease in the surface area from 409 to 362 m^2 g^{-1} after a longer TOS of 936 h, reflecting that the SiO_2 binder can inhibit coke formation during catalysis, in line with the weight loss measured by TG.

Fig. 2 displays the HAADF-STEM and EDX elemental-mapping images of the fresh and spent Ni/LaY-Al_2O_3 and Ni/LaY-SiO_2 catalysts. No clear boundaries have been visualized between zeolites and binders, confirming the thoroughly mixed zeolite and binders for all the samples. For the fresh Ni/LaY-Al_2O_3 catalyst, the average Ni particle size is determined to be ca. 24 nm, which is much larger than the average pore size of ca. 5.6 nm for Ni/LaY-Al_2O_3 (Table 1 and Fig.S3), indicating major Ni particles distributed on the external surface of the zeolites. Additionally, Ni species appear in accordance with Al distribution, indicating a strong interaction between Ni species and the Al_2O_3 binder. For the fresh Ni/LaY-SiO_2 catalyst, the average Ni particle size is similar and 23 nm, in accordance with XRD results. Notably, the spent Ni/LaY-Al_2O_3 shows an obviously increased mean Ni particle size (~40 nm) after a TOS of 156 h, as well as the aggregation of big Ni particles evidenced by EDX. In contrast, the spent Ni/LaY-SiO_2 exhibits an average Ni particle size of around 25 nm, and the intact Ni size reflects a limited Ni agglomeration for Ni/LaY-SiO_2 even after a TOS of 936 h. This is again completely consistent with the XRD results.

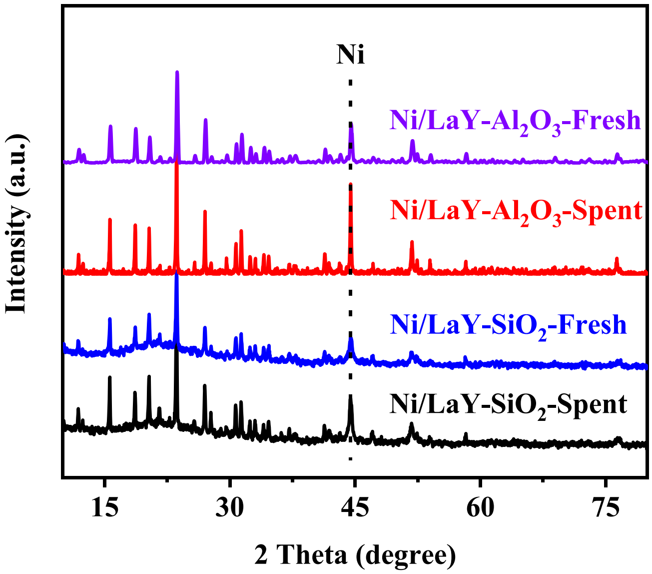

Fig. 1. XRD patterns of the fresh and spent Ni/LaY-Al_2O_3 and Ni/LaY-SiO_2 catalysts.

3.2. *Catalytic performance*

The catalytic performances of Ni/LaY-Al_2O_3 and Ni/LaY-SiO_2 catalysts for the hydrogenation of GVL were assessed over a continuous fixed-bed reactor under the conditions of $t = 200$ °C and $P_{H2} = 30$ bar. The feedstock is 45 wt% GVL in 45 wt% MeOH and 10 wt% H_2O with a WHSV of 1 h^{-1}. The yields of MP versus TOS over different catalysts are depicted in Fig. 3. For the Ni/LaY-Al_2O_3 catalyst, GVL conversion maintained around 99% within a TOS of 156 h. However, the MP yields gradually decrease from 85% to 75% within 156 h, indicating a gradual deactivation in terms of catalytic selectivity towards MP during continuous catalysis. In contrast, a complete GVL conversion and an MP yield of >93% could be sustained for Ni/LaY-SiO_2 within a TOS of 936 h, indicating the excellent durability of Ni/LaY-SiO_2 due to no apparent catalyst deactivation during the continuous and long-term catalysis. The distinct performances of two catalysts with different binders indicate that the binder could affect the catalytic performance markedly in the hydrogenation of biomass-derived platform molecule GVL. Changes to the Ni phase and the support, such as deactivation by Ni agglomeration, coke formation, and support dealumination can be expected for catalyst deactivation. In an effort to unravel the insights into the impact of the binder on catalyst performance, especially for stability, catalyst deactivation reasons should be further studied with the concerns of all above by characterizing the fresh and spent catalysts systematically.

3.3. *Insights into catalyst stability*

Changes to the Ni phase were first studied by XRD, STEM, and ICP-OES to quantitatively analyze the sintering or leaching of Ni (Fig. 1–2 and Table 1). Severe sintering of Ni particles was detected for the spent Ni/LaY-Al_2O_3, with a particle size increase from 24 to 39 nm after a continuous TOS of 156 h, as confirmed by XRD and STEM. In contrast, limited Ni sintering was shown for the spent Ni/LaY-SiO_2, with a particle size increase only from 23 to 25 nm even after a 6-fold increase in the reaction time (a TOS of 936 h). Besides, the ICP-OES results in Table 1 evidence that loss of Ni to the solvents was marginal for both two catalysts.

The acid sites are recognized to be the active sites for the GVL ring-opening step, which is recognized as the key step in the catalytic hydrogenation of GVL [15,18,32,33]. Thus, the acidic properties of the fresh and spent Ni/LaY-Al_2O_3 and Ni/LaY-SiO_2 catalysts were analyzed and quantified by NH_3-TPD and solid-state ^{27}Al MAS NMR (Fig. 4). The NH_3-TPD profiles could be divided into two regions, assigned to the weak and strong acid sites, respectively [34–36]. For Ni/LaY-Al_2O_3, a drop in the total acid amount from 853 to 716 μmol g^{-1}, was detected after a TOS of 156 h along with a major decrease in the strong acid amount from 528 to 407 μmol g^{-1}. The major decrease in the strong acid site amount should be caused by factors such as active site blockage by coke deposition and loss of active sites by support dealumination. Again, this is consistent with the apparent decrease in surface area and more coke deposition observed for the spent Ni/LaY-Al_2O_3, as shown in Table 1 and Fig. 5. In contrast, the fresh Ni/LaY-SiO_2 catalyst shows a

Table 1
Physic-chemical properties of fresh and spent Ni/LaY-Al_2O_3 and Ni/LaY-SiO_2 catalysts.

Catalyst	Metal contents (wt%)[a]			S_{BET}[b]	V_{micro}[c]	S_{micro}[c]	D_{pore}[d]	Ni particle size[e]
	Ni	Al	La	(m^2 g^{-1})	(cm^2 g^{-1})	(m^3 g^{-1})	(nm)	(nm)
Ni/LaY-Al_2O_3-Fresh	8.1	18.5	8.2	481	0.21	405	5.6	24 ± 5
Ni/LaY-SiO_2-Fresh	8.3	8.0	8.4	409	0.18	352	9.4	23 ± 6
Ni/LaY-Al_2O_3-Spent	8.0	15.9	8.6	378	0.16	323	9.0	39 ± 8
Ni/LaY-SiO_2-Spent	8.4	7.8	8.3	362	0.14	286	9.0	25 ± 4

[a] Measured by ICP-OES.
[b] Calculated by Brunauer-Emmett-Teller (BET) method.
[c] Calculated by t-plot method.
[d] Calculated by BJH method.
[e] The average particle size of Ni was derived from the STEM images in Fig. 2 with measurements of over 200 particles.

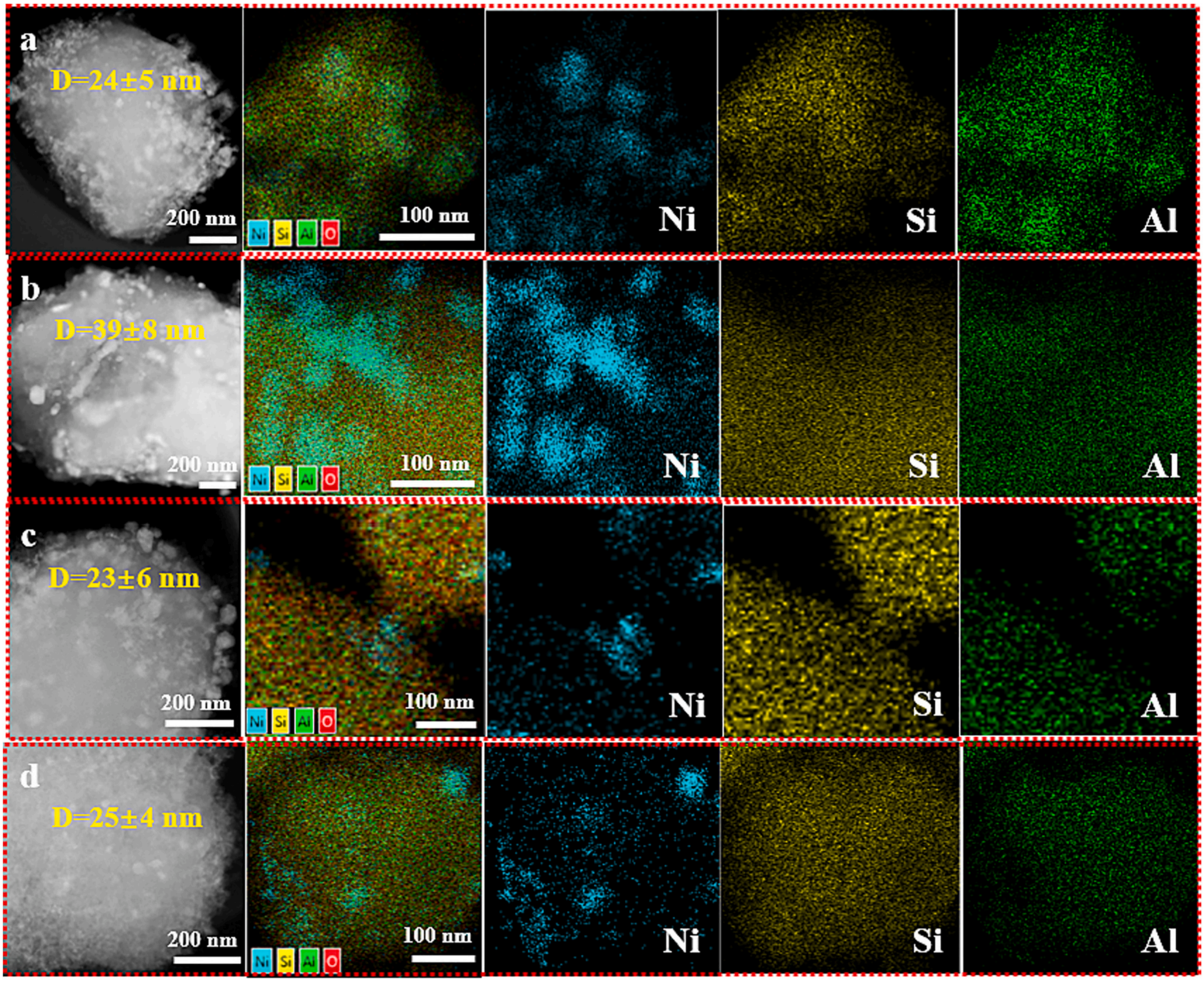

Fig. 2. Representative high-angle annular dark-field scanning transmission electron microscopy (HAADF-STEM) and corresponding EDX elemental-mapping images of the (a) fresh Ni/LaY-Al_2O_3, (b) spent Ni/LaY-Al_2O_3, (c) fresh Ni/LaY-SiO_2 and (d) spent Ni/LaY-SiO_2 catalysts (D: the average particle size).

lower total acid amount (663 μmol g^{-1}) due to the neutral properties of the silica binder. Notably, marginal changes in the acid amount (630 μmol g^{-1}) and site distribution can be observed even after a TOS of 936 h, reflecting the excellent durability of Ni/LaY-SiO_2.

The solid-state ^{27}Al MAS NMR spectra of the fresh and spent Ni/LaY-Al_2O_3 and Ni/LaY-SiO_2 catalysts are depicted in Fig. 4b. For both Ni/LaY-Al_2O_3 and Ni/LaY-SiO_2 catalysts, three resonances i.e., the tetrahedral framework aluminum (FAl) (Al_{IV}) at an isotropic shift of ca. 57 ppm, the five-coordinated extra-framework aluminum (EFAl) (Al_V) at an isotropic shift of ca. 30 ppm, and octahedral EFAl species (Al_{VI}) at an isotropic shift of about 0 ppm were detected [37–40]. For checking the extent of dealumination, the relative amounts of different Al species normalized to the Al content in the fresh catalyst as determined by ^{27}Al MAS NMR. For Ni/LaY-Al_2O_3, the content of Al_{IV}, Al_V and Al_{VI} species

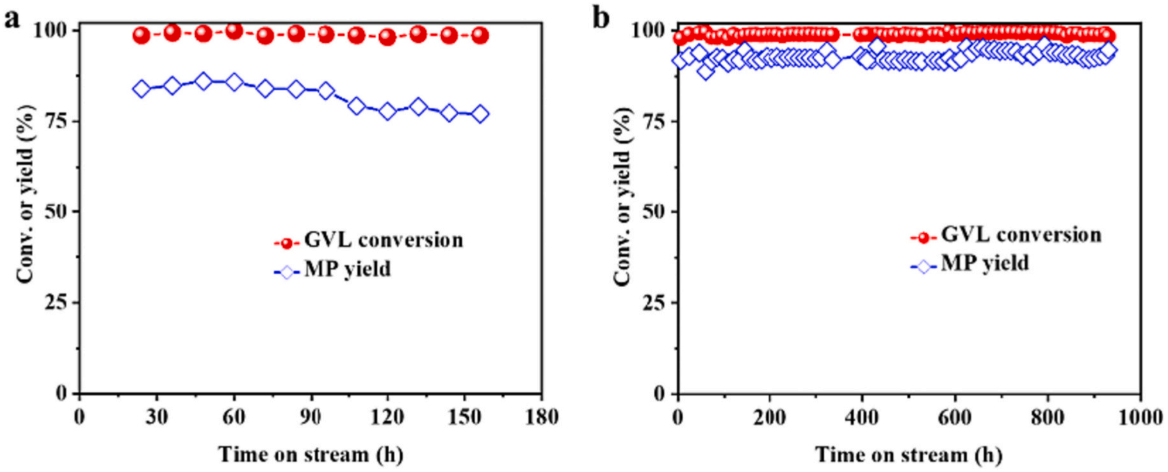

Fig. 3. Time profiles of catalytic hydrogenation of 45 wt% GVL in methanol (45%) and water (10%) over (a) Ni/LaY-Al_2O_3 and (b) Ni/LaY-SiO_2 catalysts. Reaction Conditions: 3 mL catalysts, 30 mL min^{-1} H_2, t = 200 °C, P_{H2} = 30 bar.

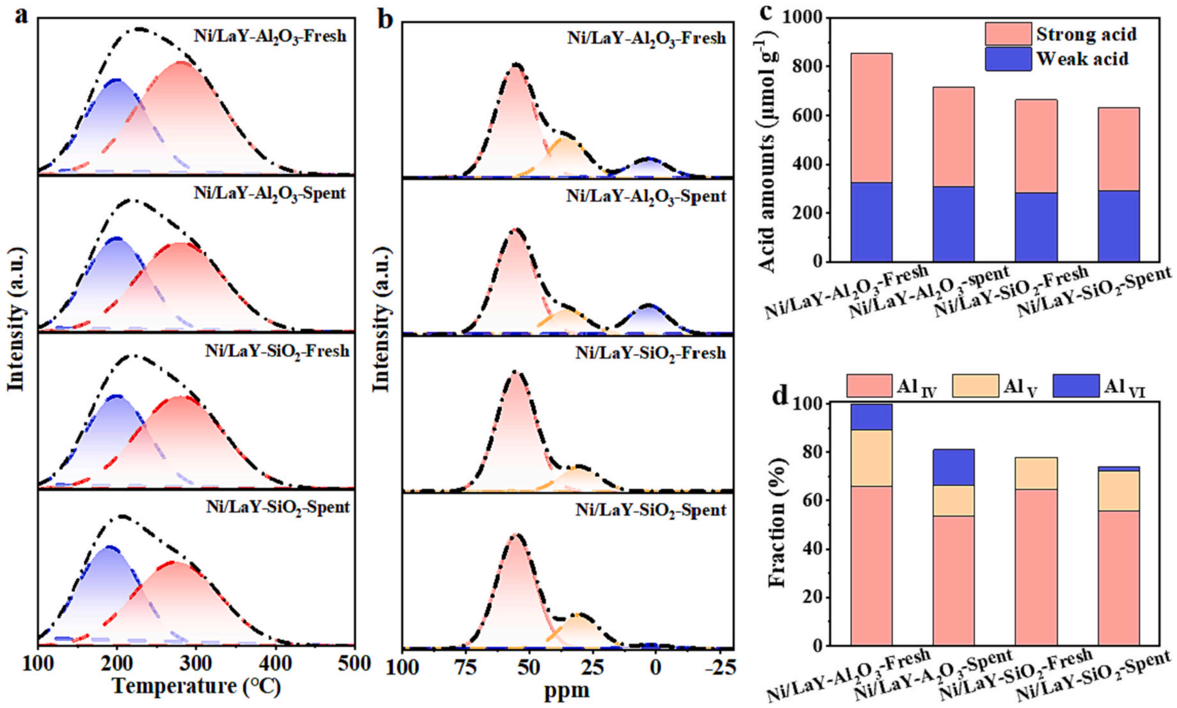

Fig. 4. (a) NH_3-TPD profiles, (b) ^{27}Al magic angle spinning nuclear magnetic resonance measurements (MAS NMR), (c) corresponding acid amounts determined by NH_3-TPD, and (d) relative amounts of Al species as determined by ^{27}Al MAS NMR of the fresh and spent Ni/LaY-Al_2O_3 and Ni/LaY-SiO_2 catalysts.

was totally decreased after catalysis. This evidences an apparent dealumination for Ni/LaY-Al_2O_3. The indication of acid site loss for Ni/LaY-Al_2O_3 after a TOS of 156 h is also consistent with the results of NH_3-TPD and ICP-OES. In contrast, a marginal change in Al_{IV} (9.2% decrease), Al_V (3.4% increase), and Al_{VI} (1.8% increase) species is observed for Ni/LaY-SiO_2 upon catalysis. Combined with a limited loss of Al species determined by ICP-OES, less severe dealumination is reflected for Ni/LaY-SiO_2 compared with that for Ni/LaY-Al_2O_3. Partial transformation of FAL into EFAL is observed for Ni/LaY-SiO_2 upon catalysis. Therefore, Ni/LaY-SiO_2 is more resistant to support dealumination compared with Ni/LaY-Al_2O_3.

Moreover, coke deposition on the spent catalysts has also been checked and determined by TG. Similar weight loss patterns of the fresh Ni/LaY-Al_2O_3 and Ni/LaY-SiO_2 catalysts are first shown in Fig. 5a, with a sharp decrease to 300 °C owing to the adsorbed species and a slow decrease up to 800 °C owing to the dehydration of hydroxyl groups in the catalysts. By comparing with the fresh counterparts, different extents of coke deposition on the spent catalysts are shown by TG measurements. More coke is deposited on the spent Ni/LaY-Al_2O_3 catalyst (3%). In contrast, the weight amount of coke is only 1.5% for the spent Ni/LaY-SiO_2 catalyst, indicating that the SiO_2 binder can efficiently alleviate coke deposition than the Al_2O_3 binder during catalysis [41–43]. To distinct the coke speciation on catalyst surface, the XPS C 1s spectra of the spent Ni/LaY-Al_2O_3 and Ni/LaY-SiO_2 catalysts were analyzed in Fig. 5b. The C 1 s signal of the spent Ni/LaY-Al_2O_3 and Ni/LaY-SiO_2 could be fitted into peaks at 284.5, 285.8 and 288.6 eV, which were

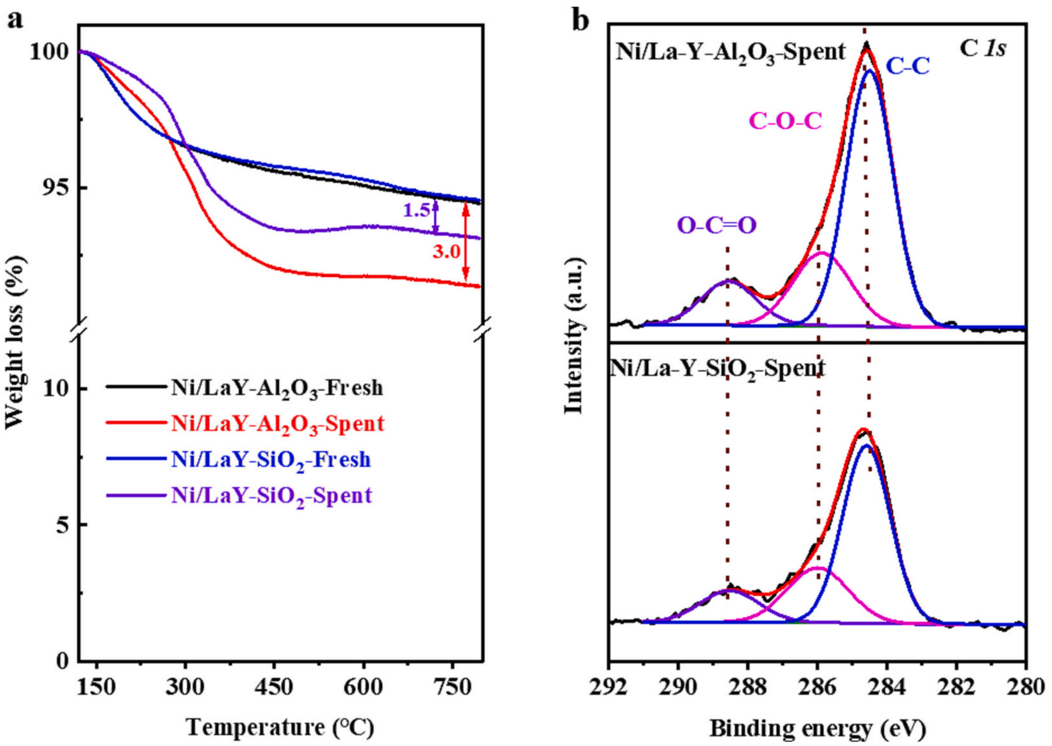

Fig. 5. (a) TG curves of the fresh and spent Ni/LaY-Al_2O_3 and Ni/LaY-SiO_2 catalysts; (b) XPS spectra of C 1s and O 1s for the spent Ni/LaY-Al_2O_3 and Ni/LaY-SiO_2 catalysts.

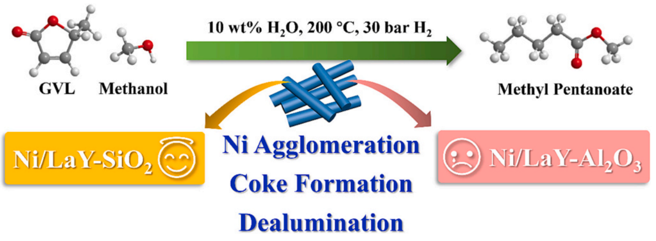

Scheme 2. Schematic illustration of the binder effect on catalyst performance in terms of stability in the continuous hydrogenation of GVL.

ascribed to graphitic-like carbon with C—C bond, residues adsorbed on the catalyst surface with C-O-C and O-C=O bonds, respectively [44–46]. The intensity of graphitic-like carbon with a C—C bond for the spent Ni/LaY-Al_2O_3 catalyst was 1.4 times higher than that of the spent Ni/LaY-SiO_2 catalyst, indicating the favorable formation of coke on Ni/LaY-Al_2O_3 during catalysis, in line with the TG results in Fig. 5a.

According to all the above results, the impact of binder selection (Al_2O_3 or SiO_2) on the catalytic performance of zeolite-based bifunctional catalysts can be revealed, as illustrated in Scheme 2. Ni/LaY-Al_2O_3 suffers more from metal sintering, coke deposition, and support dealumination during the catalytic hydrogenation of GVL into MP, which is associated with the loss/blockage of active sites and the continuous loss of acid sites. Contrastly, Ni/LaY-SiO_2 markedly improves the catalyst stability in the catalytic hydrogenation of GVL into MP. The employment of the SiO_2 binder for Ni/LaY-SiO_2 can efficiently suppress Ni agglomeration, coke deposition and support dealumination upon catalysis.

4. Conclusions

In this work, we have synthesized two zeolite-based bifunctional catalysts (Ni/LaY-Al_2O_3 and Ni/LaY-SiO_2) by extruding LaY zeolite with the selection of alumina or silica as binder and a subsequent Ni addition by the wet impregnation method. In comparison with Ni/LaY-Al_2O_3, Ni/LaY-SiO_2 possesses highly enhanced catalyst durability under practical continuous and liquid-phase hydrogenation of GVL into pentanoic esters. Ni/LaY-SiO_2 catalysts could retain a $>$ 93% MP yield even after a TOS of 936 h at 200 °C and 30 bar H_2, together with the presence of 10 wt% H_2O; while Ni/LaY-Al_2O_3 shows a gradually declined MP yield within a TOS of 156 h. Systematical characterizations with a combination of multiple techniques disclose the positive impacts of the employment of SiO_2 as a binder on enhancing the catalyst durability of zeolite-based bifunctional catalysts. The employment of a SiO_2 binder for Ni/LaY-SiO_2 can efficiently mitigate Ni agglomeration, coke deposition and support dealumination upon long-term biomass catalysis, compared with the employment of an Al_2O_3 binder for Ni/LaY-Al_2O_3. This work greatly aids the design of industrial-level bifunctional catalysts with enhanced catalyst durability, which could show great potential and create opportunities for the industrial production of pentanoic biofuels.

CRediT authorship contribution statement

Jinfei Lu: Writing – original draft, Conceptualization. **Shaohua Wang:** Data curation. **Yanheng Hao:** Formal analysis, Data curation. **Lu Lin:** Investigation. **Fan Bai:** Formal analysis. **Juan Wang:** Funding acquisition. **Qingda An:** Writing – review & editing. **Peng Tian:** Software. **Jifeng Pang:** Writing – review & editing, Funding acquisition. **Wenhao Luo:** Writing – review & editing, Supervision, Funding acquisition.

Declaration of competing interest

The authors declare that they have no competing financial interests that could have appeared to influence the work reported in this paper.

Data availability

Data will be made available on request.

Acknowledgments

National Natural Science Foundation of China (22078316 and 22378383), the Funding of Inner Mongolia University (10000-23112101/081), and Inner Mongolia Youth Science and Technology Talents (NJYT24019) are acknowledged for financial support.

Appendix A. Supplementary data

Supplementary data to this article can be found online at https://doi.org/10.1016/j.catcom.2024.106892.

References

[1] H.L. van Soest, M.G.J. den Elzen, D.P. van Vuuren, Net-zero emission targets for major emitting countries consistent with the Paris agreement, Nat. Commun. 12 (2021) 2140, https://doi.org/10.1038/s41467-021-22294-x.

[2] D. Tilman, C. Balzer, J. Hill, B.L. Befort, Global food demand and the sustainable intensification of agriculture, Proc. Natl. Acad. Sci. U. S. A. 108 (2011) 20260–20264, https://doi.org/10.1073/pnas.1116437108.

[3] B. Zhang, B.K. Biswal, J. Zhang, R. Balasubramanian, Hydrothermal treatment of biomass feedstocks for sustainable production of chemicals, fuels, and materials: progress and perspectives, Chem. Rev. 123 (2023) 7193–7294, https://doi.org/10.1021/acs.chemrev.2c00673.

[4] H.L. van Soest, M.G.J. den Elzen, D.P. van Vuuren, Net-zero emission targets for major emitting countries consistent with the Paris agreement, Nat. Commun. 12 (2021) 2140, https://doi.org/10.1038/s41467-021-22294-x.

[5] B. Zhang, B.K. Biswal, J. Zhang, R. Balasubramanian, Hydrothermal treatment of biomass feedstocks for sustainable production of chemicals, fuels, and materials: progress and perspectives, Chem. Rev. 123 (2023) 7193–7294, https://doi.org/10.1021/acs.chemrev.2c00673.

[6] D. Chiaramonti, M. Bonini, E. Fratini, G. Tondi, K. Gartner, A.V. Bridgwater, H. P. Grimm, I. Soldaini, A. Webster, P. Baglioni, Development of emulsions from biomass pyrolysis liquid and diesel and their use in engines—Part 1 : emulsion production, Biomass Bioenergy 25 (2003) 85–99, https://doi.org/10.1016/s0961-9534(02)00183-6.

[7] G.W. Huber, S. Iborra, A. Corma, Synthesis of transportation fuels from biomass: chemistry, catalysts, and engineering, Chem. Rev. 106 (2006) 4044–4098, https://doi.org/10.1021/cr068360d.

[8] R. Gérardy, D.P. Debecker, J. Estager, P. Luis, J.-C.M. Monbaliu, Continuous flow upgrading of selected C2–C6 platform chemicals derived from biomass, Chem. Rev. 120 (2020) 7219–7347, https://doi.org/10.1021/acs.chemrev.9b00846.

[9] K. Lee, Y. Jing, Y. Wang, N. Yan, A unified view on catalytic conversion of biomass and waste plastics, Nat. Rev. Chem. 6 (2022) 635–652, https://doi.org/10.1038/s41570-022-00411-8.

[10] G. Yao, G. Wu, W. Dai, N. Guan, L. Li, Hydrodeoxygenation of lignin-derived phenolic compounds over bi-functional Ru/H-Beta under mild conditions, Fuel 150 (2015) 175–183, https://doi.org/10.1016/j.fuel.2015.02.035.

[11] J.-P. Lange, R. Price, P.M. Ayoub, J. Louis, L. Petrus, L. Clarke, H. Gosselink, Valeric biofuels: a platform of cellulosic transportation fuels, Angew. Chem. Int. Ed. 49 (2010) 4479–4483, https://doi.org/10.1002/anie.201000655.

[12] K.G. Martínez Figueredo, D.J. Segobia, N.M. Bertero, Influence of the preparation method on the performance of Ni-based bifunctional catalysts in the one-pot conversion of γ-valerolactone to valeric biofuel, Catal. Commun. 144 (2020) 106087, https://doi.org/10.1016/j.catcom.2020.106087.

[13] T. Pan, J. Deng, Q. Xu, Y. Xu, Q.-X. Guo, Y. Fu, Catalytic conversion of biomass-derived levulinic acid to valerate esters as oxygenated fuels using supported ruthenium catalysts, Green Chem. 15 (2013) 2967–2974, https://doi.org/10.1039/C3GC40927A.

[14] P. Sun, G. Gao, Z. Zhao, C. Xia, F. Li, Stabilization of cobalt catalysts by embedment for efficient production of valeric biofuel, ACS Catal. 4 (2014) 4136–4142, https://doi.org/10.1021/cs501409s.

[15] W. Luo, P.C.A. Bruijnincx, B.M. Weckhuysen, Selective, one-pot catalytic conversion of levulinic acid to pentanoic acid over Ru/H-ZSM5, J. Catal. 320 (2014) 33–41, https://doi.org/10.1016/j.jcat.2014.09.014.

[16] P. Sun, G. Gao, Z. Zhao, C. Xia, F. Li, Acidity-regulation for enhancing the stability of Ni/HZSM-5 catalyst for valeric biofuel production, Appl. Catal. B Environ. 189 (2016) 19–25, https://doi.org/10.1016/j.apcatb.2016.02.026.

[17] Z. Yi, D. Hu, H. Xu, Z. Wu, M. Zhang, K. Yan, Metal regulating the highly selective synthesis of gamma-valerolactone and valeric biofuels from biomass-derived levulinic acid, Fuel 259 (2020) 116208, https://doi.org/10.1016/j.fuel.2019.116208.

[18] J. He, Z. Wu, Q. Gu, Y. Liu, S. Chu, S. Chen, Y. Zhang, B. Yang, T. Chen, A. Wang, B. M. Weckhuysen, T. Zhang, W. Luo, Zeolite-tailored active site proximity for the efficient production of pentanoic biofuels, Angew. Chem. Int. Ed. 60 (2021) 23713–23721, https://doi.org/10.1002/anie.202108170.

[19] J. He, L. Lin, M. Liu, C. Miao, Z. Wu, R. Chen, S. Chen, T. Chen, Y. Su, T. Zhang, W. Luo, A durable Ni/La-Y catalyst for efficient hydrogenation of γ-valerolactone into pentanoic biofuels, J. Energy Chem. 70 (2022) 347–355, https://doi.org/10.1016/j.jechem.2022.02.011.

[20] S. Wang, W. Cui, C. Miao, N. Tang, L. Lin, Z. Wu, Q. An, P. Tian, J. Pang, W. Luo, Efficient hydrodeoxygenation of methyl levulinate into pentanoic biofuels over Ru/USY catalysts, Dalton Trans. 52 (2023) 7405–7410, https://doi.org/10.1039/D3DT01169K.

[21] J. He, L. Lin, W. Luo, The revitalization of 'the closer the better' in zeolite-tailored bifunctional catalysts for biomass valorization, ChemCatChem 14 (2022), https://doi.org/10.1002/cctc.202200728.

[22] G.T. Whiting, F. Meirer, M.M. Mertens, A.-J. Bons, B.M. Weiss, P.A. Stevens, E. de Smit, B.M. Weckhuysen, Binder effects in SiO_2 and Al_2O_3-bound zeolite ZSM-5-based extrudates as studied by microspectroscopy, ChemCatChem 7 (2015) 1312–1321, https://doi.org/10.1002/cctc.201402897.

[23] G.T. Whiting, S.-H. Chung, D. Stosic, A.D. Chowdhury, L.I. van der Wal, D. Fu, J. Zecevic, A. Travert, K. Houben, M. Baldus, B.M. Weckhuysen, Multiscale mechanistic insights of shaped catalyst body formulations and their impact on catalytic properties, ACS Catal. 9 (2019) 4792–4803, https://doi.org/10.1021/acscatal.9b00151.

[24] N.-L. Michels, S. Mitchell, J. Pérez-Ramírez, Effects of binders on the performance of shaped hierarchical MFI zeolites in methanol-to-hydrocarbons, ACS Catal. 4 (2014) 2409–2417, https://doi.org/10.1021/cs500353b.

[25] K. Kennes, A. Kubarev, C. Demaret, L. Treps, O. Delpoux, M. Rivallan, E. Guillon, A. Méthivier, T. de Bruin, A. Gomez, B. Harbuzaru, M.B.J. Roeffaers, C. Chizallet, Multiscale visualization and quantification of the effect of binders on the acidity of shaped zeolites, ACS Catal. 12 (2022) 6794–6808, https://doi.org/10.1021/acscatal.2c02152.

[26] M. Rivera-Torrente, D. Kroon, M.-V. Coulet, C. Marquez, N. Nikolopoulos, R. Hardian, S. Bourrelly, D. De Vos, G.T. Whiting, B.M. Weckhuysen, Understanding the effects of binders in gas sorption and acidity of aluminium fumarate extrudates, Chem. Eur. J. 28 (2022) e202103420, https://doi.org/10.1002/chem.202103420.

[27] X. Du, X. Kong, L. Chen, Influence of binder on catalytic performance of Ni/HZSM-5 for hydrodeoxygenation of cyclohexanone, Catal. Commun. 45 (2014) 109–113, https://doi.org/10.1016/j.catcom.2013.10.042.

[28] X.-D. Chen, X.-G. Li, H. Li, J.-J. Han, W.-D. Xiao, Interaction between binder and high silica HZSM-5 zeolite for methanol to olefins reactions, Chem. Eng. Sci. 192 (2018) 1081–1090, https://doi.org/10.1016/j.ces.2018.08.047.

[29] S. Guo, S. Yu, H. Tian, Z. Da, Mechanistic insights into the interaction between binders and Y-type zeolites in fluid catalytic cracking, Fuel 324 (2022) 124640, https://doi.org/10.1016/j.fuel.2022.124640.

[30] M. Wang, Q. Xie, H. Chen, G. Liu, X. Cui, L. Jiang, Surface regulated Ni nanoparticles on N-doped mesoporous carbon as an efficient electrocatalyst for CO_2 reduction, Chin. J. Catal. 42 (2021) 2306–2312, https://doi.org/10.1016/S1872-2067(21)63903-7.

[31] Y. Wang, H. Wang, J. Han, Q. Ge, X. Zhu, Enhancing direct deoxygenation of m-cresol to toluene through inhibiting C-C hydrogenolysis via alloying Ni with Cu, Chem. Eng. Res. Des. 199 (2023) 49–60, https://doi.org/10.1016/j.cherd.2023.09.023.

[32] W. Luo, W. Cao, P.C.A. Bruijnincx, L. Lin, A. Wang, T. Zhang, Zeolite-supported metal catalysts for selective hydrodeoxygenation of biomass-derived platform molecules, Green Chem. 21 (2019) 3744–3768, https://doi.org/10.1039/C9GC01216H.

[33] W. Luo, U. Deka, A.M. Beale, E.R.H. van Eck, P.C.A. Bruijnincx, B.M. Weckhuysen, Ruthenium-catalyzed hydrogenation of levulinic acid: influence of the support and solvent on catalyst selectivity and stability, J. Catal. 301 (2013) 175–186, https://doi.org/10.1016/j.jcat.2013.02.003.

[34] N. Karanwal, D. Verma, P. Butolia, S.M. Kim, J. Kim, One-pot direct conversion of levulinic acid into high-yield valeric acid over a highly stable bimetallic Nb-Cu/Zr-doped porous silica catalyst, Green Chem. 22 (2020) 766–787, https://doi.org/10.1039/C9GC03516H.

[35] W. Dai, L. Zhang, R. Liu, G. Wu, N. Guan, L. Li, Plate-like ZSM-5 zeolites as robust catalysts for the cracking of hydrocarbons, ACS Appl. Mater. Interfaces 14 (2022) 11415–11424, https://doi.org/10.1021/acsami.1c23614.

[36] G. Wu, N. Zhang, W. Dai, N. Guan, L. Li, Construction of bifunctional co/H-ZSM-5 catalysts for the hydrodeoxygenation of stearic acid to diesel-range alkanes, ChemSusChem 11 (2018) 2179–2188, https://doi.org/10.1002/cssc.201800670.

[37] M. Ravi, V.L. Sushkevich, J.A. van Bokhoven, Towards a better understanding of Lewis acidic aluminium in zeolites, Nat. Mater. 19 (2020) 1047–1056, https://doi.org/10.1038/s41563-020-0751-3.

[38] K. Chen, Z. Gan, S. Horstmeier, J.L. White, Distribution of aluminum species in zeolite catalysts: ^{27}Al NMR of framework, partially-coordinated framework, and non-framework moieties, J. Am. Chem. Soc. 143 (2021) 6669–6680, https://doi.org/10.1021/jacs.1c02361.

[39] J.L. Mancuso, V. Van Speybroeck, The nature of extraframework aluminum species and Brønsted acid site interactions under catalytic operating conditions, J. Catal. 429 (2024) 115211, https://doi.org/10.1016/j.jcat.2023.115211.

[40] W. Luo, E.R.H. van Eck, P.C.A. Bruijnincx, B.M. Weckhuysen, Influence of levulinic acid hydrogenation on aluminum coordination in zeolite-supported ruthenium

catalysts: A ^{27}Al 3QMAS nuclear magnetic resonance study, ChemPhysChem 19 (2018) 379–385, https://doi.org/10.1002/cphc.201700785.

[41] F.M. Almulla, S.A. Ali, M.R. Aldossary, E.I. Alnaimi, V.I. Zholobenko, A.B. Jumah, A.A. Garforth, On the influence of alumina as a binder on the performance of Pt-Beta catalyst during the transalkylation of toluene and 1,2,4-Trimethylbenzene, Microporous Mesoporous Mater. 320 (2021) 111095, https://doi.org/10.1016/j.micromeso.2021.111095.

[42] A. Ebrahimi, M. Haghighi, S. Aghamohammadi, Single vs. dual-binder surface design of spray-dried Si–Al-sol-bound kaolin-matrixed SAPO-34 nanocatalyst for conversion of methanol to light-olefins in fluidized bed reactor, Microporous Mesoporous Mater. 332 (2022) 111714, https://doi.org/10.1016/j.micromeso.2022.111714.

[43] J.S.J. Hargreaves, A.L. Munnoch, A survey of the influence of binders in zeolite catalysis, Catal. Sci. Technol. 3 (2013) 1165, https://doi.org/10.1039/c3cy20866d.

[44] L. An, C. Dong, Y. Yang, J. Zhang, L. He, The influence of Ni loading on coke formation in steam reforming of acetic acid, Renew. Energy 36 (2011) 930–935, https://doi.org/10.1016/j.renene.2010.08.029.

[45] S. Li, Y. Qi, Y. Tang, H. Jubaer, B. Dai, S. Zhou, Q. Liu, Z. Chen, Y. Zhu, H. Song, L. Zhang, Non-destructive characterisation of coke deposit on FCC catalyst and its transient evolution upon air-firing and oxy-fuel regeneration, Chem. Eng. J. 430 (2022) 132998, https://doi.org/10.1016/j.cej.2021.132998.

[46] W. Cao, W. Luo, H. Ge, Y. Su, A. Wang, T. Zhang, UiO-66 derived Ru/ZrO_2@C as a highly stable catalyst for hydrogenation of levulinic acid to γ-valerolactone, Green Chem. 19 (2017) 2201–2211, https://doi.org/10.1039/c7gc00512a.